*M. Bitou, M. Okamoto**

Advanced Polymeric Nanostructured Materials Engineering, Graduate School of Engineering Toyota Technological Institute, Nagoya, Japan

Fabrication of Porous 3-D Structure from Poly(L-lactide)-based Nanocomposite Foam via Enzymatic Degradation

In order to prepare the porous three-dimensional (3-D) structure in biodegradable polyester materials we have conducted the enzymatic degradation of a poly(L-lactide) (PLLA)-based nano-composite foam having nanocellular structure, using proteinase-K as a degrading agent at 37 °C. The surface and cross sectional morphologies of the foam recovered after enzymatic hydrolysis for different intervals were investigated by using scanning electron microscope. The nanocelluar took up large amount of water, which led to the swelling of the foam due to the large surface area inside the nanocelluar structure, and facilitated the enzymatic degradation of matrix PLLA as compared with the bulk (pre-foamed) sample. Consequently, we have successfully prepared a porous 3-D structure as a remaining scaffold in the core part of the nano-composite foam, reflecting the spherulite of the crystallized PLLA.

1 Introduction

Over the last few years, the utility of inorganic nanoscale particles as filler to enhance the polymer performance has been established. Of particular interest is recently developed nanocomposite technology consisting of a polymer and organically modified layered filler (organo-clay) because they often exhibit remarkably improved mechanical and various other materials properties as compared with those of virgin polymer or conventional composite (micro/macro-composites) (Sinha Ray and Okamoto, 2003a; Vaia and Wagner, 2004; Gao, 2004; Okamoto, 2006; Okada and Usuki, 2006; Hussain et al., 2006). These concurrent property improvement are well beyond what can be generally achieved through the micro/macro-composites preparation.

In our recent publications, we have reported on the preparation, characterization, mechanical and various other materials properties (Sinha Ray et al., 2002a, 2003b, 2003c, 2003d), biodegradability (Sinha Ray et al., 2002b, 2002c, 2003e), melt rheology (Sinha Ray et al., 2003b; 2003f), crystallization behavior (Nam et al., 2003) and finally foam processing (Shinh Ray et al., 2003f; Fujimoto et al., 2003) of a series of poly(L-lactide) (PLLA)-based nano-composites. In all cases intrinsic properties of pure PLLA were concurrently improved after nano-composites preparation. Thus, these materials hold very strong future promise for potential applications as high-performance biodegradable materials, and open a new dimension for plastics and composites (Sinha Ray and Okamoto, 2003g).

Most recently, further study has examined the morphological correlation between the dispersed organo-clay particles with nanometer dimensions in the bulk and the formed closed- and/or open-cellular structure after foaming (Ema, et al., 2006). The incorporation with nano-clay induced heterogeneous nucleation because of a lower activation energy barrier compared with homogeneous nucleation as revealed by the characterization of the interfacial tension between bubble and matrix. The grown cells having diameter of ~ 200 nm were localized along the dispersed nano-clay particles in the cell wall. The dispersed nano-clay particles acted as nucleating sites for cell formation and the cell growth occured on the surfaces of the clays. The nano-composites provided excellent nano-composite foams having high cell density from microcellular to nanocellular.

The nanocellular structure has a potential applications as a fabrication of porous three-dimensional (3-D) structure for tissue engineering scaffolds (Hoedle et al., 2001). In the fabrication of the porous 3-D structure, an open-cell structure must be generated because an appropriate cell size and porosity promotes cell infiltration and controlled drug release matrixes (Coombes and Meikle, 1994). Several methods have been reported to prepare porous biodegradable polymeric materials by the removal of one component from binary phase-separated biodegradable polyester blends by the water-extraction for PLLA/poly(ethylene oxide) blends (Tsuji et al., 2000) and the selective enzymatic degradation for PLLA/poly(ε-caprolactone) blends (Tsuji and Ishizaka, 2001). Hsiue in Wang et al. (2005) ■ reported that the fabrication of the porous sphere structure based on crystalline PLLA via enzymatic degradation of PLLA-block-poly(2-ethyl-2-oxazoline) (PEOz)-block-PLLA triblock copolymer, where the PEOz-block is water-soluble

* Mail address: M. Okamoto, Advanced Polymeric Nanostructured Materials Engineering, Graduate School of Engineering Toyota Technological Institute, 2-12-1 Hisakata, Tempaku, Nagoya 4688511, Japan
E-mail: okamoto@toyota-ti.ac.jp

IPP_ipp2073 – 14.9.07/druckhaus köthen

polyrlectrolyte, using the enzyme proteinase-K (Wang et al., 2005). The enzymatic degradation has a potential to be utilized as the fabrication of the porous 3-D structure, and also progresses on the surface of materials because of the heterogeneous reaction between the water-insoluble PLLA polymer chains and water-soluble enzyme macromolecules. Therefore, the enzymatic hydrolysis of PLLA-phases proceeds through surface erosion mechanism (Tsuji and Ishizaka, 2001). That is, specific surface area plays a decisive role in the degradation process.

In this aspect, the enzyme-catalyzed hydrolysis of PLLA-based nano-composite foams having high cell density is expected to produce the porous 3-D structure in biodegradable polyester materials.

To understand the enzymatic degradation behavior of PLLA-based nano-composite foams, we have to know the degradation behavior of the nano-composites having different degree of crystallinity in the presence of organo-clay particles in detail.

In this study, we conducted the enzymatic degradation of PLLA matrix before and after nano-composites preparation, using proteinase-K as a degrading agent. We also discuss here the enzymatic degradation of the nano-composite foam having nanocellular structure.

2 Experimental Section

2.1 Nano-composite Preparation

A commercial poly(L-lactide) (PLLA) with a D content of 1.1 to 1.7 % ($M_w = 133 \times 10^3$ g mol^{-1}, $M_w/M_n = 1.58$, $T_g \sim 60$ °C and $T_m \sim 169$ °C) supplied by Unitika Co. Ltd., Japan was dried under vacuum at 60 °C, and kept under dry nitrogen gas for one week prior to use. The organically modified clay (organo-clay) used in this study were synthesized by replacing Na^+ ions in montmorillonite (MMT) with octadecylammonium cations (Sinha Ray et al., 2003d; Fujimoto et al., 2003). The mean interlayer spacing of the (001) plane (d_{001}) for the organo-MMT powder was 2.31 nm (Fujimoto et al., 2003). Nano-composite was prepared by melt extrusion at 210 °C. The details of the nanocomposites preparation were described in our previous papers (Sinha Ray et al., 2003d). The nano-composite prepared with 5 wt.% organo-clay was denoted as PLLACN5. The strands were pelletized and dried under vacuum at 60 °C for 48 h to remove water. The dried PLLACN5 pellets were converted into sheets with a thickness of 0.18 and 0.88 mm by pressing with ~ 1.5 MPa at 190 °C for 3 min using a hot press. The molded sheets were quickly quenched between glass plates and then annealed at 100 °C for 7 min up to 10 h to crystallize isothermally before being subjected to various characterizations and foam processing.

2.2 Foam Processing

Foam processing of PLLACN5 was conducted in an autoclave (TSC-WC-0096, Taiatsu Techno Co) by using supercritical CO_2 (Ema et al., 2006). Crystallized nano-composite sheet ($10 \times 25 \times 0.88$ mm^3 = width × length × thickness) was inserted into an autoclave (96 mL) and CO_2 pressure was increased up to 28 MPa at 100 °C for 4 h. For such a long time of CO_2 dissolution into the sample, CO_2 has already been completely saturated in the sample at fixed temperature. Subsequently, the CO_2 was quickly released from the autoclave (within 3 s). After releasing the CO_2 pressure, the formed foam was stabilized *via* cooling by liquid-CO_2 to room temperature, and then removed carefully from the autoclave and kept at ambient temperature.

The mass density of both pre-foamed (ρ_p) (= 1.2620 g/cm^3) and post-foamed (ρ_f) in g/cm^3 samples were estimated by using the buoyancy method. The average cell radius (d) in mm was determined from the data of scanning electron microscope (SEM) observation. The sample almost obeyed the Gaussian distribution. The function for determining cell density (N_c) in cell/cm^3 is defined as the following Eq. 1 (Ema et al., 2006)

$$N_c = 10^4 \frac{3[1 - (\rho_f/\rho_p)]}{4\pi d^3}. \quad (1)$$

On the other hand, the mean cell wall thickness (δ) in μm was estimated by the following equation (Eq. 2) (Ema et al., 2006).

$$\delta = d\left(\sqrt{1 - (\rho_f/\rho_p)} - 1\right). \quad (2)$$

2.3 Enzymatic Degradation

The enzymatic degradation of neat PLLA and PLLACN5 having different crystallinity in the presence of proteinase-K was conducted according to the procedure reported by Reeve et al. (1994).

The film ($10 \times 25 \times 0.18$ mm^3 = width × length × thickness) was placed in a vial filled with 5 mL of 100 mM Tris-HCL buffered solution (Nacalai Tesque) (pH 7.9) containing 0.2 mg/mL proteinase-K (Nacalai Tesque, lyophilized powder, 36.9 units/mg) and then incubated at a thermosta-controlled temperature of 37 °C in a shaker for up to 240 h. For the degradation of nano-composite foam, we used thick film (sheet) ($10 \times 25 \times 0.88$ mm^3 = width × length × thickness) instead of thin film sample. The foam was incubated for 1000 h. The hydrolysis media were changed every 24 h to maintain enzymatic activity. Specimens were withdrawn at certain intervals, and washed with distilled water to stop further enzymatic hydrolysis and then dried under vacuum at room temperature for two days prior to the characterization. All measurements were performed for three replicates of specimens and averaged to get the final result.

The enzymatic degradation rate of the specimens were estimated by the weight loss and normalized weight loss using the following equation:

$$\text{Weight loss } (\mu g/mm^2) = \left(\frac{W(t=0) - W(t)}{A_0}\right)\left(\frac{x_{PLLA}}{(V_{PLLA})^{2/3}}\right), \quad (3)$$

$$\text{Normalized weight loss } (\%) = \left(\frac{W(t=0) - W(t)}{W(t=0)}\right), \quad (4)$$

where W(t = 0), W(t) and A_0 are the film weights before and after hydrolysis and intial surface area of the films, respectively. x_{PLLA} and V_{PLLA} correspond to wt. and volume fractions of PLLA in each sample on the assumption that the ratio of

Parameters	Neat PLLA	PLLACN5
$M_w \times 10^{-3}/g \cdot mol^{-1}$	133	121
M_w/M_n	1.58	2.21
T_m/°C	169.4	165.1
T_g/°C	60	59.2
χ_c/%	49.9	46.1

Table 1. Characteristic Parameters of neat PLLA and PLLACN5

PLLA/organo-MMT removed from the films is the same as that before degradation.

For the hydrolysis of nano-composite foam, we also evaluated the water absorption by the following equation.

$$\text{Water absorption (wt.\%)} = \left(\frac{W(\text{wet}) - W(t)}{W(t)}\right), \quad (5)$$

where W (wet) is the wet weight of a specimen after degradation.

2.4 Characterization

2.4.1 Gel Permeation Chromatography (GPC)

The weight-average (M_w) and number-average (M_n) molecular weights of neat PLLA and PLLACN5 were determined from GPC (LC-VP, Shimadzu Co.), using polystyrene standards for calibration and tetrahydrofuran (THF) as the carrier solvent at 40 °C with a flow rate of 0.5 mL/min. For the GPC measurements first PLLA or PLLACN5 were dissolved in chloroform and then diluted with THF (Fujimoto et al., 2003).

GPC results of PLLA in pure state or organo-clay filled system are presented in Table 1. As anticipated, the incorporation of organo-clay resulted in a reduction in the molecular weight of the PLLA matrix. Decreased molecular weights of PLLA in PLLACN5 may be explained by either the shear mixing of PLLA and organo-clay or the presence of ammonium salt, both resulting in a certain degree of hydrolysis of PLLA matrix at high temperature.

2.4.2 Differential Scanning Calorimetric (DSC)

The crystallized specimens were characterized by using temperature-modulated DSC (TMDSC) (TA 2920; TA Instruments) at the heating rate of 5 °C/min with a heating/cooling cycle of the modulation period of 60 s and an amplitude of +/−0.769 °C, to determine the melting temperature (T_m) and heat of fusion, the DSC was calibrated with Indium before experiments (Sinha Ray et al., 2003c).

For the measurement of degree of crystallinity (χ_c) prior to TMDSC analysis, the extra heat absorbed by the crystallites formed during heating had to be subtracted from the total endothermic heat flow due to the melting of the whole crystallites. This can be done according to the principles and procedures described in our previous paper (Nam et al., 2001). In the TMDSC experiments (see Fig. 6), the endothermic heat flow $\Delta H_{different}$ of the initially existing crystallites can be easily calculated as $\Delta H_{difference} = \Delta H_{rev} - \Delta H_{nonrev}$, where ΔH_{rev} is the endothermic melting (reversing) enthalpy from the reversing heat flow profile and ΔH_{nonrev} is the exothermic ordering/crystallization (nonreversing) enthalpy from the nonreversing heat flow profile appearing in the temperature range of −30 to 200 °C. The χ_c was thus calculated as $\Delta H_{difference}/\Delta H^0$ with $\Delta H^0 = 93$ J/g, which is the melting enthalpy of 100 % crystalline PLLA (Fisher et al., 1973) (see Table 2).

System	Time/min	$\Delta H_{difference}$	χ_c /%
Neat PLLA	0	0.02	0.02
	20	9.70	10.4
	30	27.9	30.0
	600	46.5	50.0
PLLACN5	0	0.05	0.05
	7	7.44	8.42
	12	16.0	18.2
	25	27.0	30.6
	30	30.3	34.3
	600	40.7	46.1

Table 2. Isothermal crystallization and degree of crystallinity (χ_c) annealed at 100 °C

2.4.3 Morphology

The cell structures were investigated by using scanning electron microscope (SEM) (JSM-5310LV, JEOL). The samples were freeze-fractured in liquid nitrogen and sputter-coated with gold at an argon pressure of 0.1 Torr for 3 min at a current of 10 mA (Fujimoto et al., 2003). The surface and cross sectional morphologies of the specimens before and after hydrolysis were also observed with a SEM. The samples were sputter-coated with gold to a thickness of ~ 20 nm.

The nanoscale structure of PLLACN5 was investigated by means of transmission electron microscopy (TEM) (H-7100, Hitachi Co.), operating at an accelerating voltage of 100 kV. The ultra thin section (the edge of the sample sheet perpendicular to the compression mold) with a thickness of 100 nm was microtomed at −80 °C using a Reichert Ultra cut cryo-ultramicrotome without staining (Reeve et al., 1994).

2.4.4 Wide-Angle X-ray Diffraction (WAXD)

WAXD analyses were performed for the organo-clay powder, neat PLLA and PLLACN5 using an Mxlabo X-ray diffractometer (MAC Science Co.; 3 kW, graphite monochromator, CuKα radiation ($\lambda_x = 0.154$ nm), operated at 40 kV and 20 mA). Samples were scanned in fixed time mode with counting time of 2 s under diffraction angle 2θ in the range 1° to 30° (Sinha Ray et al., 2003d; Fujimoto et al., 2003).

3 Results and Discussion

3.1 Nano-composite Structure

Fig. 1 shows the results of TEM bright field images of PLLACN5 having $\chi_c = 46.1$ %, in which dark entities are the

IPP_ipp2073 – 14.9.07/druckhaus köthen

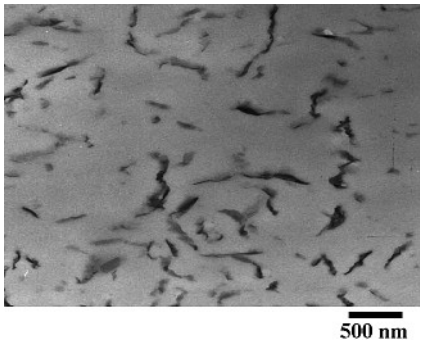

Fig. 1. Bright filed TEM images of PLLA-based nano-composite (PLLACN5). The dark entities are the cross section and/or face of intercalated-and-stacked silicate layers and the bright areas are the matrix

cross section of intercalated MMT layers. From the TEM images it becomes clear that there are some intercalated-and-stacked silicate layers in the nano-composites.

We estimate the form factors obtained from TEM images, the average value of the length (L) of the dispersed particles and the correlation length (ξ) between them (Sinha Ray et al., 2003d). From the WAXD patterns, the crystallite size (D) of intercalated-and-stacked MMT layers of PLLACN5 is calculated by using the Scherrer equation (Sinha Ray et al., 2003d). The calculated value of D ($\cong$ thickness of the dispersed particles) and other parameters for the nano-composite are presented in Table 3.

PLLACN5 exhibits a large value of L (450 ± 200 nm) with a large level of stacking of the silicate layers (D ~ 21nm) suggesting that the intercalated MMT layers are homogeneously and finely dispersed in PLLA matrix. Because ξ value of this nano-composite is same order of magnitude compared with the value of L. The number of the stacked individual silicate layers ($\equiv D/d_{001} + 1$) is about 8. WAXD patterns and TEM observation respectively established that well ordered intercalated nano-composite was formed in case of PLLACN5. Details regarding structural analysis can be found in our previous publication (Yoshida and Okamoto, 2006).

3.2 Enzymatic Degradation of PLLACN5

In enzymatic degradation, Williams (1981) reported the hydrolysis of PLLA in the presence of proteinase-K, which was successfully extracted from protease in a fungus called *Tritirachium album* in 1974. This enzyme has a molecular weight of 18 500 ± 500, an isoelectric point of 8.9 and a pH optimum activity range between 7.5 and 12.0 (Ebeling et al., 1974). Proteinase-K preferentially degrades PLLA over poly(D-lactide). The degradation rate significantly increases with reducing % L content from 100 to 92 % in PLLA, suggesting the crystalline order dominates enzymatic degradation (Reeve et al., 1994).

Parameters	PLLACN5
d_{001}/nm[a]	3.03
D/nm[b]	20.9
$(D/d_{001}) + 1$	7.9
L/nm	450 ± 200
ξ/nm	260 ± 140
L/D	22 ± 9

[a] d_{001} for organo-MMT is equal to 2.31 nm.
[b] The value is calculated by using the Scherrer equation

Table 3. Form factors of PLLACN5 obtained from WAXD and TEM observations

Fig. 2 shows the time variation of the weight (in $\mu g/mm^2$) and normalized weight losses (in %) of PLLCN5 having different χ_c during the enzymatic degradation. Obviously, the weight losses increase linearly with degradation time (t) over a period of 250 h, (corresponding to 90 wt.% degradation for amorphous PLLACN5), regardless of χ_c in the matrix PLLA. On the other hand, we can observe an induction period, which is onset time until start of the weight loss in the specimen. The induction time becomes longer with increasing χ_c in the film. To elucidate the degradation mechanism of the nano-composite, the linear degradation rate is estimated from the slope (d[weight loss]/dt) in the linear regime, as indicated by the solid line (χ_c = 34.3 %) in Fig. 2A, and is plotted as a function of the initial χ_c of the film prior to hydrolysis in Fig. 4. For com-

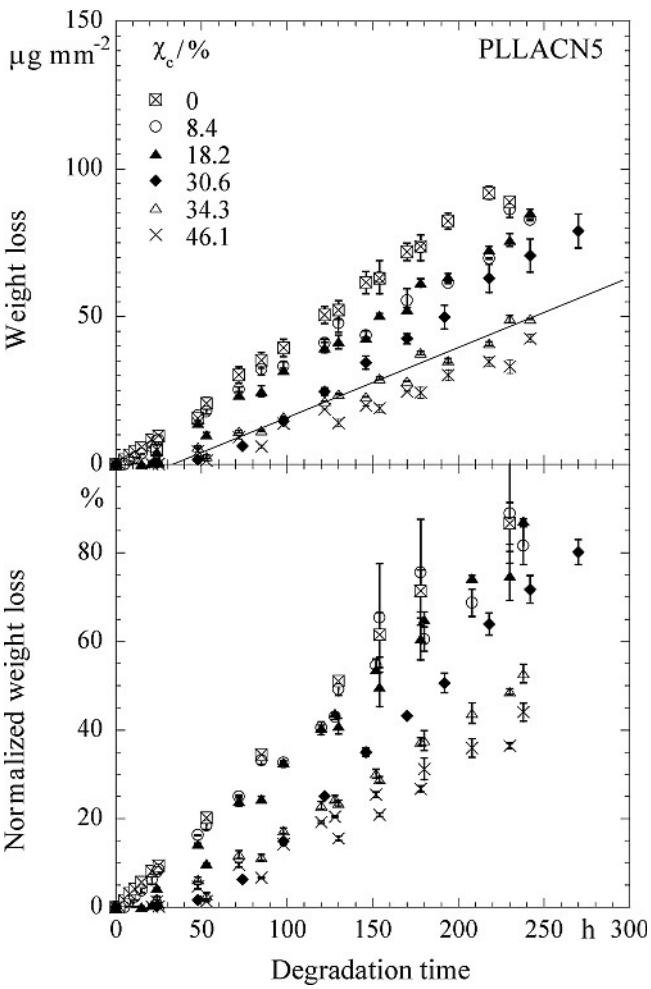

Fig. 2. Weight loss (A) and normalized weight loss (B) of PLLACN5 with different χ_c during the enzymatic degradation. The solid line in (A) is calculated by linear regression

parison, we also conducted the hydrolysis experiment of neat PLLA with different χ_c in the film specimens (Fig. 3). The same feature has been observed in PLLA degradation in the results of various χ_c as compared with the nano-composite degradation. When an amorphous PLLA film was exposed beyond 200 h the complete film disappearance was observed without any residual solid particle, suggesting the PLLA was completely degradable by proteinase-K to water-soluble products, i. e., lactic acid (LA) monomer and LA-LA dimer, and LA-LA-LA trimer on the basis of high-performance liquid chromatography (HPLC) analysis as reported by Abe et al. (Reeve et al., 1994; Iwata and Doi, 1998; Abe et al., 1997). The specimens incubated over identical exposure condition without proteinase-K exhibited no measurable weight loss. This indicates that the weight loss solely occurs by the enzyme-catalyzed process and the subsequent release of MMT particles into the surrounding media. For amorphous PLLACN5 film incubated for 240 h, the organo-MMT particles were migrated as a precipitate to the bottom of the vial.

The linear degradation rates of PLLACN5 and PLLA having different χ_c are shown in Fig. 4, and the induction time is summarized in Fig. 5. For both PLLACN5 and PLLA, the degradation rate slightly decreases with increasing initial χ_c in the range of 0–30 %. However, the rate abruptly decreases beyond χ_c = 30 %. For better understanding, a previous reported result on the enzymatic degradation of neat PLLA ($M_w = 3 \times 10^5$) (Tsuji and Miyauchi, 2001) with high χ_c values is also added in this plot. The dispersed MMT layers have almost no effect on the acceleration of the degradation rate in the enzymatic hydrolysis of PLLACN5. This observation suggests that the linear degradation rate of PLLACN5 is affected by the initial value of χ_c as well as neat PLLA degradation reported by several researchers (Reeve et al., 1994; Iwata and Doi, 1998; Abe et al., 1997; Tsuji and Miyauchi, 2001). The enzymatic hydrolysis of matrix PLLA proceeds preferentially at disordered amorphous region on the sample surface rather than the restricted amorphous domains, which are located between the crystalline

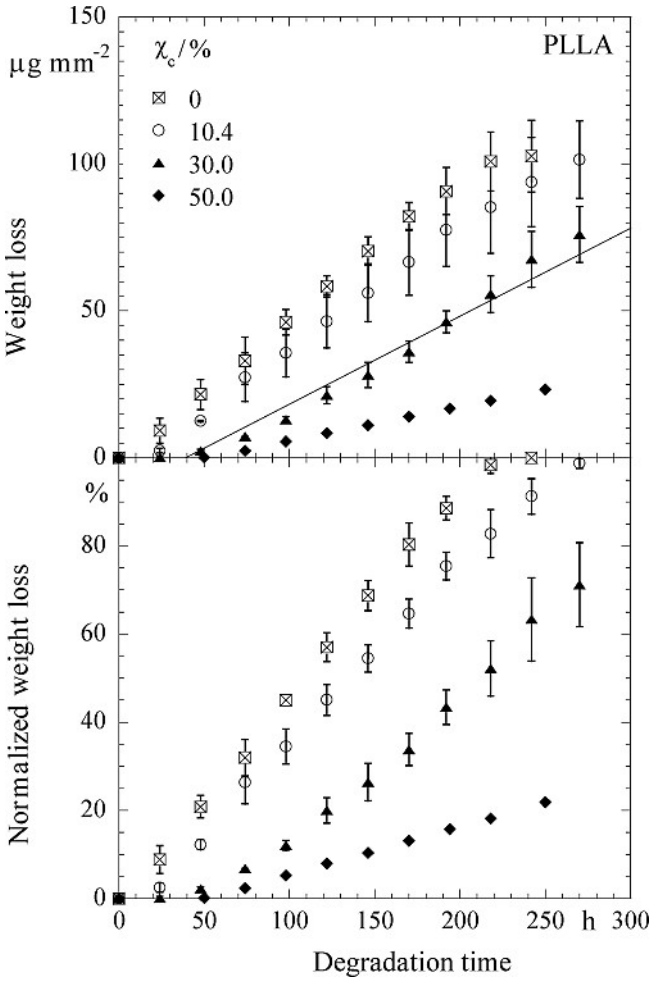

Fig 3. Weight loss (A) and normalized weight loss (B) of PLLA with different χ_c during the enzymatic degradation. The solid line in (A) is calculated by linear regression

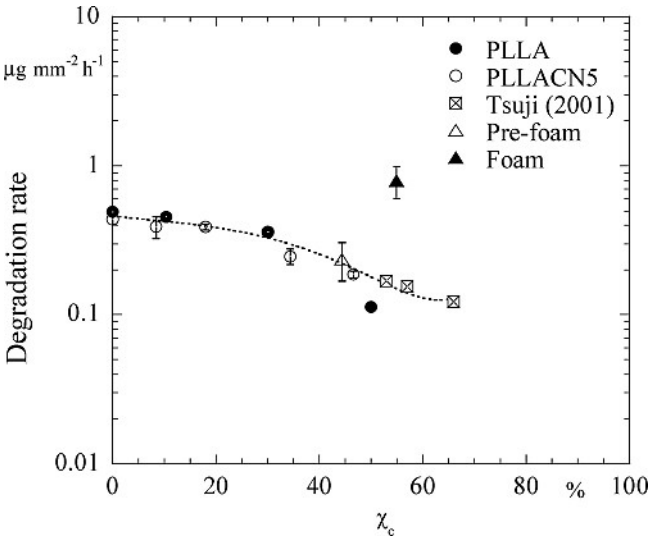

Fig. 4. Semi-logarithmic plots of linear degradation rates (μg/mm² h) of PLLACN5 (bulk), nanocelluar foam and PLLA (bulk) versus initial χ_c. A previous results on PLLA (bulk) with high χ_c values are reproduced from reference (Tsuji and Miyauchi, 2001)

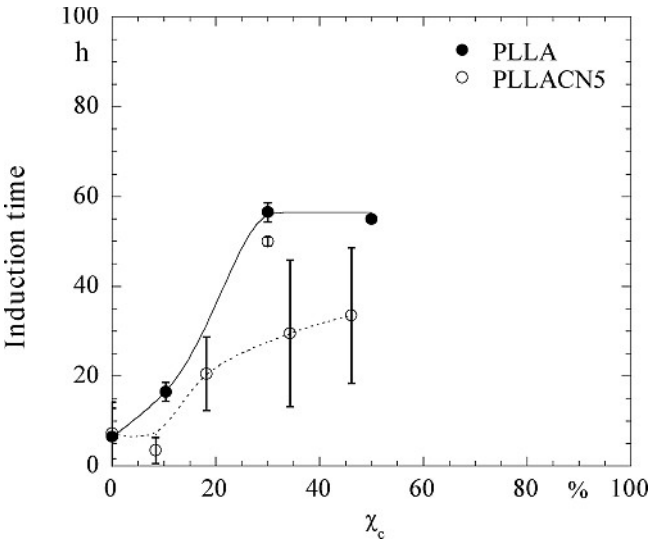

Fig. 5. Plots of induction time versus initial χ_c

IPP_ipp2073 – 14.9.07/druckhaus köthen

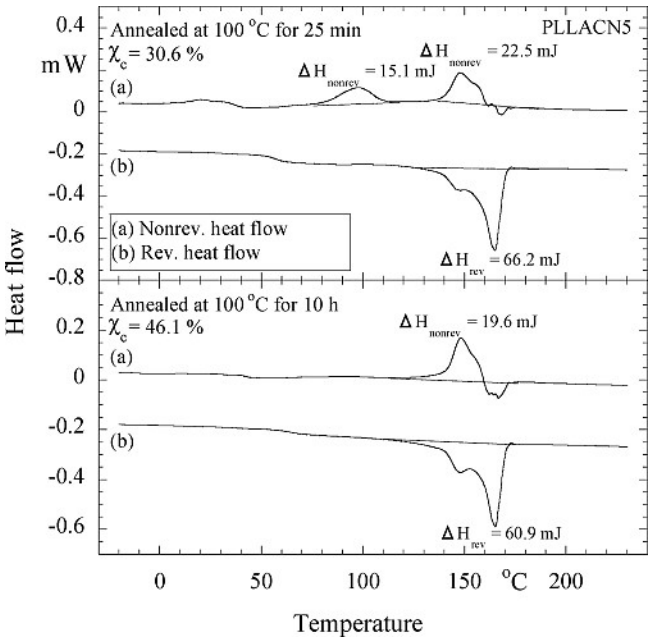

Fig. 6. TMDSC scan for PLLACN5 with different χ_c values: (a) nonreversing heat flow and (b) reversing heat flow

lamellae in the spherulites (Tsuji and Miyauchi, 2001). The degradation rate is strongly affected by the disappearance of the free amorphous regions. This feature is also observed in the rapid increasing of the induction time (see Fig. 5).

As seen in Fig. 6, the TMDSC thermogram of the PLLACN5 with χ_c = 30.6 % exhibits the existence of the free amorphous region outside the spherulites as revealed by the appearance of the recrystallization peak in the temperature range of 70 to 120 °C. In contrast, for PLLACN5 with χ_c = 46.1 % such extra heat absorbed by the recrystallization does not show in the profile. The nonreverse heat flow at temperature range of 120 to 170 °C accompanied with a small remnant melting around 147 °C in reverse heat flow, corresponding to the phase transition from α' modification (left-handed 10/3 helices) to α structure (left-handed 3/1 helices) (Zhang et al., 2005).

3.3 Enzymatic Degradation of Nano-composite Foam

Fig. 7A shows the results of SEM images of the fracture surface (cross cection) of the PLLACN5 foamed at 100 °C (before degradation). We noted here that the foam exhibit nicely the closed-cell structure and homogeneous cells distribution, suggesting that the dispersed silicate particles act as nucleating sites for cell formation (Ema et al., 2006). The nano-composite foams nicely obeyed the Gaussian distribution. We have quantitatively calculated various morphological parameters of the foam: these are summarized in Table 4.

As reported by many researchers (Tsuji et al., 2000; Williams, 1981; Iwata and Doi, 1998; Tsuji and Miyauchi, 2001), the enzymatic degradation of matrix PLLA proceeds through surface erosion mechanism. In this process, the enzyme can not diffuse into the film bulk. However, in the case of foam having nanocellular structure, the enzyme can contact with a lot of polymer chains at the cell wall surface compared with

Parameters	PLLACN5 Foam
ρ_f/g cm^{-3} [a]	1.010
d/nm	165
$N_c \times 10^{-12}$/cell cm^{-3}	3.83
δ/nm	410
d/ξ	0.63
d/L	0.36
δ/L	0.91

[a] ρ_p for PLLACN5 is 1.2620 g cm^{-3}

Table 4. Morphological parameters of PLLACN5 foam

that of pre-foamed sample. Fig. 8 presents the weight loss data of thick film sample of PLLACN5 (pre-foamed, χ_c = 44.4 %) and post-foamed sample (χ_c = 54.5 %). The linear degradation rate was in the range of 0.6–1.0 μg/mm^2 h for the foam and 0.17 to 0.3 μg/mm^2 h for the pre-foam, as presented in Fig. 4. This fact suggests that the linear degradation rate of the nanocomposite foam is about five times higher than that of neat PLLA with same crystallinity. The accelerated enzymatic degradation in the foam is caused by the large surface area inside the nanocelluar structure. From Table 4, the calculated value of the specific surface area (3.6×10^5 mm^2) was three order of magnitude higher than that of PLLA bulk (320 mm^2). This feature is assigned to the observation in water uptake data (Fig. 9). The nano-composite foam appears much more water uptake than the bulk. During the first 250 h, the water absorption of the foam increases continuously to attain 50 %. Beyond 300 h, the water uptake remains almost constant, presumably due to the saturation caused by the morphology development after enzymatic degradation. That is, the water can more easily penetrate into the foam. In contrast, PLLACN5 bulk shows very hydrophobic less than 2 % of absorbed water during the degradation period. The nanocelluar takes up large amount of water, which lead to the swelling of the foam, and thus facilitate the enzymatic degradation of matrix PLLA as compared with the pre-foamed sample. The content of absorbed water greatly determines the enzymatic degradability.

3.4 Morphological Change during Enzymatic Degradation

Fig. 7 shows the cross section and the surface morphologies of the nano-composite foam recovered after enzymatic degradation for different time intervals. For comparison, the surface morphologies of the pre-foamed sample (PLLACN5 bulk) were also investigeted by using SEM. The surfaces of both foamed and pre-foamed samples are smooth before degradation (Fig. 7D and G). For the pre-foamed sample, a lot of pores are generated on the surface after degradation up to 120 h and the pores with diameter of ~ 3 μm are spherical in shape with circular interconnections (Fig. 7G to I). This kind of connected spherical-pore structure has been widely reported in the previous papers (Li et al., 2001; Cai et al., 2003). These holes are resulted from the degradation of the swollen (amorphous) region by the enzymatic attacks (Fukuda et al., 2002).

In contrast, for the foamed sample, there is a great tendency to generate the skin-layer (~ 100 μm thickness) with cracked

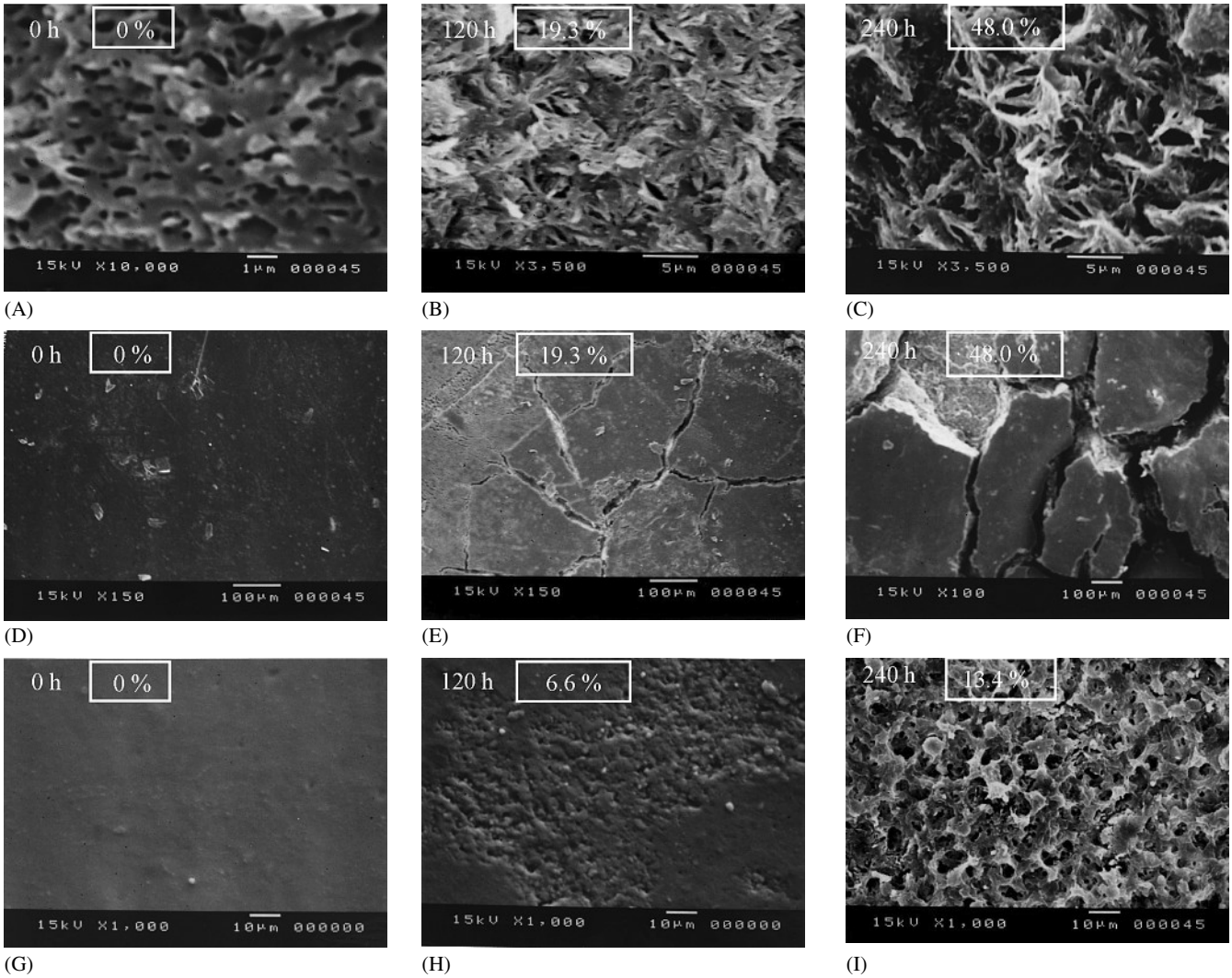

Fig. 7. Typical results of SEM images of the cross section and the surface of nano-composite foam , A to C (cross section), D to F (surface), and pre-foam (bulk) G to I (surface) after enzymatic degradation for different time intervals. The weight loss (in %) of each specimen is shown by the number in the box

surface and hence more rapid fragmentation on the surface (Fig. 7F). No significant change, such as pore formation, on the surface during degradation up to 120 h suggests that the core part of the foam underwent significant hydrolysis during this period. This indicates that the cell structure allows the PLLA chains to become susceptible to enzymatic hydrolysis. This speculation is supported by the water uptake behavior of the foam.

Fig. 7A to C present the morphological change of the cross section in the foam after enzymatic degradation for different time intervals. Interestingly, after degradation of 120 h, the sample has some flower-like structure (Wang et al., 2005) as a remaining scaffold in the core part, reflecting the spherulite of the crystallized PLLA. After the restricted amorphous region has been degraded, the porous 3-D scaffold left the core part in the foam. This morphology of the PLLA crystals is enhanced with degradation up to 240 h. The structure size with a diameter of 10 µm observed by SEM is in good agreement with the average diameter of the spherulite developed in the sample by annealing at 100 °C before degradation (Nam et al., 2003). The generation of the porous 3-D structure is completely different from the enzymatic degradation of bulk sample, where the morphology of the core parts remain unchanged during degradation because of the surface erosion mechanism (photo not shown). Thus, the degraded nano-composite foam provides the porous 3-D scaffold and the pore size is determined by controlling the degradation time using proteinase-K as an effective degrading agent.

3.5 Change in the Thermal Properties and Molecular Weights

Fig. 10 summarizes the results of the thermal properties, i. e., T_m and χ_c of the residual sample recovered after degradation. T_m of the pre-foamed sample always remains constant at the initial temperature, accompanied with a very small increase in χ_c. For the core part of the foam after degradation, T_m remains almost constant value until 20 % in weight loss, beyond which it decreases rapidly to 162.6 °C at weight loss of 30 %, accompanying a small increase in χ_c. On the other hand, the monoto-

IPP_ipp2073 – 14.9.07/druckhaus köthen

nous decrease in T_m takes place and χ_c becomes as large as 90 % in the skin part of the foamed sample after degradation of 430 h, corresponding to the weight loss in 54.3 %. The crystalline lammellae (folding PLLA chains) exhibit the hydrolysis-resistance of the chains in the folding surfaces, which provide a very slow rate of degradation. Therefore, a large increase in χ_c is due to the preferential enzymatic degradation in the restricted amorphous region, leaving the crystalline residue. The depression in T_m may be explained by the variation of the thickness of crystalline lamellae [(Tsuji and Miyauchi, 2001). T_m must decrease linearly with reciprocal lamellar thickness (Gedde, 1995). At this moment, we are not able to propose the real mechanism of T_m depression. Such discussion is beyond the objective of this paper, and we will report it separately.

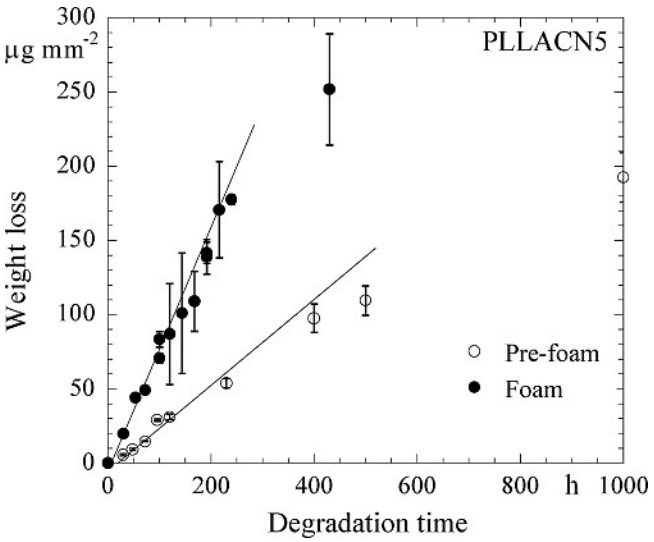

Fig. 8. Time dependence of weight loss of bulk PLLACN5 (pre-foam) with χ_c = 44.4 % and foam with χ_c = 54.5 % during the enzymatic degradation. The solid lines for the degradation period of 0 to 250 h are calculated by linear regression

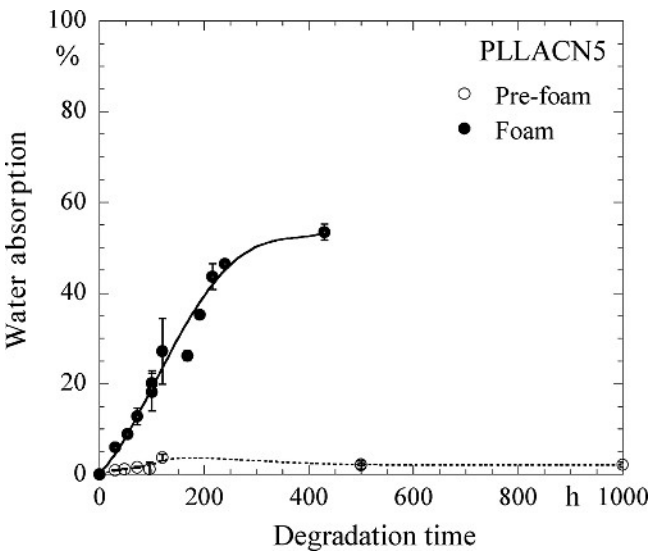

Fig. 9. Water absorption changes of PLLACN5 (pre-foam) and foam during the enzymatic degradation at 37 °C

The residual samples of both core and skin parts after enzyme exposure times of variable duration were also analyzed by GPC. After a weight loss of 20 %, both residual PLLAs show little change in M_w. The large decreased M_w in the core and skin part was observed beyond degradation of 192 h ($M_w = 98 \times 10^3$ g mol^{-1}, $M_w/M_n = 3.04$ for core part and $M_w = 14 \times 10^3$ g mol^{-1}, $M_w/M_n = 1.67$ for skin part) (weight loss in 30 %). This is in agreement with the characteristics of enzymatic degradation of bulk PLLA (Reeve et al., 1994; Iwata and Doi, 1998; Tsuji and Miyauchi, 2001), i. e., weight loss without molecular weight decrease.

Further studies are currently in progress to elucidate the mechanism and characteristics of the enzymatic degradation of various nano-composite foams having different cell size.

4 Conclusions

In this study, we have demonstrated the enzymatic degradation of PLLA matrix before and after nano-composites preparation, using proteinase-K as a degrading agent. The dispersed MMT layers had almost no effect on the acceleration of the degrada-

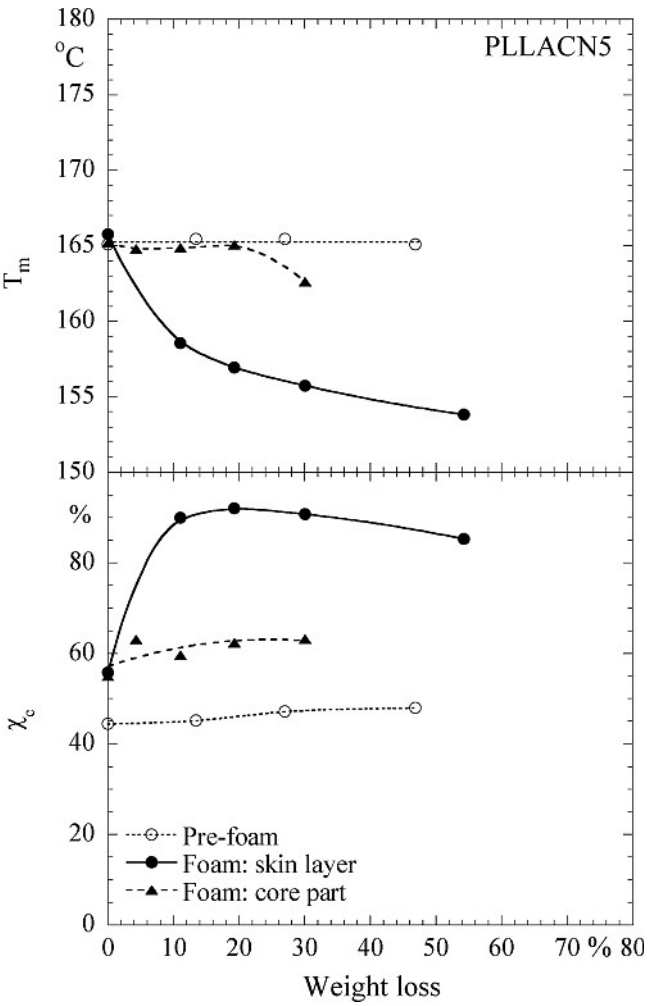

Fig. 10. Plots of T_m (A) and χ_c (B) for the residual sample recovered after enzyme exposure times of variable duration

tion rate in the enzymatic hydrolysis of PLLACN5. The linear degradation rate of PLLACN5 was affected by the initial value of χ_c as well as neat PLLA degradation. In contrast, the linear degradation rate of the nano-composite foam was about five times higher than that of neat PLLA with same crystallinity. In the foam, the accelerated enzymatic degradation was caused by the large surface area inside the nanocelluar structure. The nanocelluar took up large amount of water, which led to the swelling of the foam, and thus facilitated the enzymatic degradation of matrix PLLA as compared with the bulk (pre-foamed) sample. The content of absorbed water greatly determined the enzymatic degradability. For this reason, we have successfully prepared a porous 3-D structure as a remaining scaffold in the core part of the nano-composite foam, reflecting the spherulite of the crystallized PLLA. Thus, the degraded nano-composite foam provided the porous 3-D scaffold and the pore size was determined by controlling the degradation time using proteinase-K as an effective degrading catalyst.

References

Sinha Ray, S., Okamoto, M., "All Titles are missing, please check our web page for Instructions to authors and deliver the references as asked for." Prog. Polym. Sci. 28, p. 1539 – ■ (2003a)
Vaia, R. A., Wagner, H. D., Materials Today 7, p. 32 – ■ (2004)
Gao, F., Materials Today 7, p. 50 – ■ (2004)
Okamoto, M., Mater. Sci. Tech. 22, p. 756 – ■ (2006)
Okada, A., Usuki, A., Macromol. Mater. Eng. 291, p. 1449 – ■ (2006)
Hussain, F., et al., J. Composite Mater. 40, p. 1511 – ■ (2006)
Sinha Ray, S., et al., Macromolecules 35, p. 3104 – ■ (2002a)
Sinha Ray, S., et al., ■ Polymer 44, p. 857 – ■ (2003b)
Sinha Ray, S., et al., Polymer 44, p. 6631 – ■ (2003c)
Sinha Ray, S., et al., Chem. Mater. 15, p. 1456 – ■ (2003d)
Sinha Ray, S., et al., Nano Lett. 2, p. 1093 – ■ (2002b)
Sinha Ray, S., et al., Macromol. Rapid. Commun. 23, p. 943 – ■ (2002c)
Sinha Ray, S., et al., Macromol. Mater. Eng. 288, p. 203 – ■ (2003e)
Sinha Ray, S., et al., Macromol. Mater. Eng. 288, p. 936 – ■ (2003f)
Nam, J. Y., et al., Macromolecules 36, p. 7126 – ■ (2003)
Fujimoto, Y., et al., Macromol. Rapid Commun. 24, p. 457 – ■ (2003)
Sinha Ray, S., Okamoto, M., Macromol. Rapid. Commun. 24, p. 815 – (2003g)
Ema, Y., et al., Polymer 47, p. 5350 – ■ (2006)
Hoedle, S. M., et al., Chem. Commun. p.109 – ■ (2001)
Coombes, A. G. A., Meikle, M. C., Clin. Mater. 17, p. 35 – ■ (1994)
Tsuji, H., et al., J. Appl. Polm. Sci. 75, p. 629 – ■ (2000)
Tsuji, H., Ishizaka, T., Macromol. Biosci. 1, p. 59 – ■ (2001)
Wang, C. H., et al., Biomaterials 26, p. 2803 – ■ (2005)
Fujimoto, Y., et al., Macromol. Rapid Commun., 24, 457 – ■ (2003)
Reeve, M. S., et al., Macromolecules 27, p. 825 – ■ (1994)
Nam, P. H., et al., Polymer 42, p. 9633 – ■ (2001)
Fisher, E. W., et al., Polymer 25, p. 980 – ■ (1973)
Yoshida, O., Okamoto, M., Macromol. Rapid Commun., 27, p. 751 – ■ (2006)
Williams, D. F., Eng. Med. 10, p. 5 – ■ (1981)
Ebeling, W. et al., Eur. J. Biochem., 47, p. 91 – ■ (1974)
Iwata, T., Doi, Y., Macromolecules 31, p. 2461 – ■ (1998)
Abe, H., et al., Polymer 39, p. 59 – ■ (1997)
Tsuji, H., Miyauchi, S., Polym. Degrad. Stab. 71, p. 415 – ■ (2001)
Zhang, J., et al., Macromolecules 38, p. 8012 – ■ (2005)
Li, S., et al., Polym. Degrad. Stab. 71, p. 61 – ■ (2001)
Cai, Q., et al., Biomaterials 24, p. 629 – ■ (2003)
Fukuda, N., et al., Polym. Degrad. Stab. 78, p. 119 – ■ (2002)
Gedde, U. W., Polymer Physics, Chapman & Hall, London (1995)

Acknowledgments

This work was supported by the MEXT "Collaboration with Local Communities" Project (2005 – 2009).

Date received: May 14, 2007
Date accepted: September 4, 2007

Bibliography
DOI 10.3139/217.2073
Intern. Polymer Processing
XXII (2007) 5; page ■–■

ISSN 0930-777X